Atmospheric Research 265 (2022) 105927

Contents lists available at ScienceDirect

Atmospheric Research

journal homepage: www.elsevier.com/locate/atmosres

Inconsistency in historical simulations and future projections of temperature and rainfall: A comparison of CMIP5 and CMIP6 models over Southeast Asia

Mohammed Magdy Hamed [a,c,*], Mohamed Salem Nashwan [b], Shamsuddin Shahid [c], Tarmizi bin Ismail [c], Xiao-jun Wang [d,e], Ashraf Dewan [f], Md Asaduzzaman [g]

[a] Construction and Building Engineering Department, College of Engineering and Technology, Arab Academy for Science, Technology and Maritime Transport (AASTMT), B 2401 Smart Village, 12577 Giza, Egypt
[b] Construction and Building Engineering Department, College of Engineering and Technology, Arab Academy for Science, Technology and Maritime Transport (AASTMT), 2033 Elhorria, Cairo, Egypt
[c] Department of Water and Environmental Engineering, School of Civil Engineering, Faculty of Engineering, Universiti Teknologi Malaysia (UTM), 81310 Skudia, Johor, Malaysia
[d] State Key Laboratory of Hydrology-Water Resources and Hydraulic Engineering, Nanjing Hydraulic Research Institute, Nanjing 210029, China
[e] Research Center for Climate Change, Ministry of Water Resources, Nanjing 210029, China
[f] Spatial Sciences Discipline, School of Earth and Planetary Sciences, Curtin University, Kent Street, Bentley, Perth 6102, Australia
[g] Department of Engineering, School of Digital, Technologies and Arts, Staffordshire University, Stoke-on-Trent, UK

ARTICLE INFO

Keywords:
Tropical climate
GCM
CMIP5/CMIP6
Uncertainty
Köppen climate classification

ABSTRACT

The objective of this research was to assess the difference in historical simulations and future projections of rainfall and temperature of CMIP5 (RCP4.5 and 8.5) and CMIP6 (SSP2–4.5 and 5–8.5) models over Southeast Asia (SEA). Monthly historical rainfall and temperature estimations of 13 global climate models common to both CMIPs were evaluated to assess their capability to reproduce the spatial distribution and seasonality of European Reanalysis (ERA) rainfall and temperature. Models were used to determine uncertainty with spatiotemporal variability of rainfall and temperature projections. The CMIP6 GCMs did not appear to perform better than the older CMIP5 in SEA unlike other parts of the globe, except for rainfall. The CMIP6 models showed Kling-Gupta Efficiency (KGE) values in the range of −0.48-0.6, 0.21-0.85 and 0.66-0.91 in simulating historical rainfall, maximum temperature and minimum temperature compared to 0.13-0.46, 0.3-0.86 and 0.42-0.92 for CMIP5. The improvement in CMIP6 models in SEA was in the low uncertainty in ensemble simulation. The projections of CMIP5 and CMIP6 showed a relatively smaller increase in temperature with the CMIP6 ensemble when compared to CMIP5 models, while rainfall appeared to decrease. The geographical distribution of the changes indicated a greater increase in temperature in the cooler region than in the warmer region. In contrast, there was increase in rainfall in the wetter region and a smaller improvement in the drier region. This indicates increased homogeneity in temperature spatial variability, but more heterogeneity in rainfall, in the SEA region under climate warming scenarios.

1. Introduction

Climate change is a global issue due to the damaging effects on various sectors, including water resources, public health, energy, and agriculture (Lee et al., 2017; Muhammad et al., 2019; Shahid, 2010; Shahid et al., 2017). Mapping possible changes in the climatic parameters is crucial for planning climate change adaptation and mitigation strategies. It is particularly important in environmentally-critical locations, where subtle changes in weather parameters may significantly impact the service sector. Global Climate Models (GCMs) have the ability to simulate the effects of greenhouse gas (GHG) emissions on climatic systems and realistically predict future conditions (Flato et al.,

* Corresponding author at: Construction and Building Engineering Department, College of Engineering and Technology, Arab Academy for Science, Technology and Maritime Transport (AASTMT), B 2401 Smart Village, 12577 Giza, Egypt.
E-mail addresses: eng.mohammedhamed@aast.edu (M.M. Hamed), m.salem@aast.edu (M.S. Nashwan), sshahid@utm.my (S. Shahid), tarmiziismail@utm.my (T. Ismail), xjwang@nhri.cn (X.-j. Wang), A.Dewan@curtin.edu.au (A. Dewan), Md.Asaduzzaman@staffs.ac.uk (M. Asaduzzaman).

https://doi.org/10.1016/j.atmosres.2021.105927
Received 4 September 2021; Received in revised form 3 November 2021; Accepted 11 November 2021
Available online 15 November 2021

2013; Hartmann, 2016). These models are widely used to model past climatic conditions and project future responses to increased GHG emissions and land-use changes (Chen et al., 2014; Taylor et al., 2011; van Vuuren et al., 2011). A major advantage of GCMs is their ability to predict future climate in response to various atmospheric GHG concentration scenarios. These GCMs are available publicly as part of the Coupled Model Intercomparison Project (CMIP).

Most GCMs incorporate a large degree of uncertainty, primarily due to inadequate model descriptions of the physical processes driving the climate system and climate scenarios (Gao et al., 2019; Hamed et al., 2021a; Weigel et al., 2010). Certain models, however, are capable of resolving regional climatic events, thereby increasing their usefulness in predicting future climate change scenarios for a given region. It is normally a good idea to utilize all available climate models to reflect a complete range of future changes. CMIP models have rigorously improved over the years to overcome these uncertainties, from CMIP1 to the latest version, CMIP6 (Eyring et al., 2016).

CMIP6 GCMs differ from previous CMIPs in that the newest version provides a more accurate depiction of the Earth's physical processes. Additionally, the CMIP6 model forecasts additional scenarios using shared socioeconomic pathways (SSPs) (O'Neill et al., 2016; Schlund et al., 2020). These updated climate projections take socioeconomic developments, technological advancement, and other environmental factors (such as land use) into account (Moss et al., 2010), enabling the development of new scenarios to better evaluate the consequences of climate change policies. CMIP6 places a premium on coordinated experiments to gain a better understanding of the processes behind climate variability. As a result, CMIP6 GCMs are expected to minimize possible bias to a greater extent than their predecessors (Arias et al., 2021; Iqbal et al., 2021; Song et al., 2021b).

Southeast Asia (SEA), located between two oceans (the Pacific to the east and the Indian to the west) and two continental regions (Asia and Australia), is considered the largest archipelago in the world (Chang et al., 2005). The climate in this region is tropical, with high temperatures and well-distributed monthly rainfall of >200 mm. The climate is determined by latent heat release near the equator and convective tropical air masses. The rainfall distribution is controlled by a land-sea breeze process, resulting from the interaction of elevated island topography and synoptic winds (Hamed et al., 2021b; Qian, 2008).

SEA has experienced different climatic extremes over the last 50 years (including droughts during El Nino events and heavy rains in La Nina periods) especially in the Indonesian region (Nasional, 2012; Dewi, 2010). The mean temperature has risen by 0.1–0.03 °C per decade over the past 50 years, and the sea level has risen by 1–3 mm per year (IPCC, 2007). The severity and frequency of climatic extremes are likely to increase, putting the SEA region at risk of climate change impacts (Thirumalai et al., 2017; Ge et al., 2019; Nashwan et al., 2018a; Raghavan et al., 2017). Significant changes in seasonal rainfall patterns and an increase in the frequency of flooding and water shortage would profoundly affect many service sectors (Nashwan et al., 2018b; Nashwan and Shahid, 2022; Ziarh et al., 2021). In order to be prepared for these increased impacts, policymakers must be informed about the climate change implications for these areas and the adaptation methods required to mitigate impacts and increase industry resilience.

Numerous studies have examined both the historical and potential future climate change in SEA and adjacent areas using GCMs (Desmet and Ngo-Duc, 2021; Iqbal et al., 2021; Kang et al., 2019; Khadka et al., 2021; McSweeney et al., 2015; Noor et al., 2019; Salman et al., 2020; Supari et al., 2020; Supharatid et al., 2021; Tangang et al., 2020). For example, Iqbal et al. (2021) used compromised programming to rank 35 CMIP6 GCMs for Mainland Southeast Asia (MSEA). Analysis revealed that three GCMs could accurately reproduce annual mean rainfall over central and southern regions. Desmet and Ngo-Duc (2021) investigated rainfall, near-surface temperature and wind for 28 CMIP6 models in SEA. They ranked GCMs by combining two different scores (spatial and temporal) to generate each variable score. A final global score, combining all variables, is then reported. Khadka et al. (2021) compared 28 CMIP5 and 32 CMIP6 GCMs to assess their ability to replicate large-scale atmospheric circulations over the SEA summer monsoon domain. These showed better performance for the CMPI6 GCMs than for CMIP5. These studies evaluated the historical performance of GCMs in regards of simulating climate over SEA. Only Supharatid et al. (2021) investigated the change in rainfall and temperature in SEA using CMIP6, although their study was confined to MSEA. They utilized two SSP scenarios to examine changes in climate parameters. It appears that a comprehensive assessment involving a comparison of CMIP5 and CMIP6 historical simulations and future projection over the entire SEA (comprising both mainland and maritime continents) is lacking. Despite the governments in this region having already taken steps to reduce climate change effects based on the CMIP5 modelling, this planning could be negatively impacted by population growth and large-scale economic development. So the risk associated with climate change would not be uniform over the whole region. Governments in the region need current, detailed information to inform the adaptation strategies selected for various SSPs. A comparative evaluation of the projections, based on CMIP5 and CMIP6 models, is essential for the region in order to streamline all existing adaptation measures.

This study aims to evaluate the difference in previous historical estimations and projections of CMIP5 and CMIP6 models over Southeast Asia. Both rainfall and temperature data are examined and evaluated to assess the validity of the decision-making process based on the various projections.

2. Description of the study area and data

2.1. Southeast Asia (SEA)

SEA lies between latitude −10°–30°N and longitude 90°–141°E (Fig. 1). SEA covers an area of about 4,550,000 km^2. It includes eleven countries and is made up of two main regions (Mainland and Maritime Southeast Asia). SEA is located within the zone of the Asian monsoon cycle, located between the Pacific and Indian Oceans. It is one of Asia's most active regions affected by convective heating processes. SEA has a generally level topography apart from some parts of Myanmar and Indonesia, where the elevation rises to 4000 m above sea level. The average yearly rainfall for the region varies between 750 and 5000 mm (Khan et al., 2019; Peel et al., 2007; Yang et al., 2021), and the mean temperature is 25 °C. As a result of the diverse spatiotemporal atmospheric processes occurring within the region, climate extremes such as

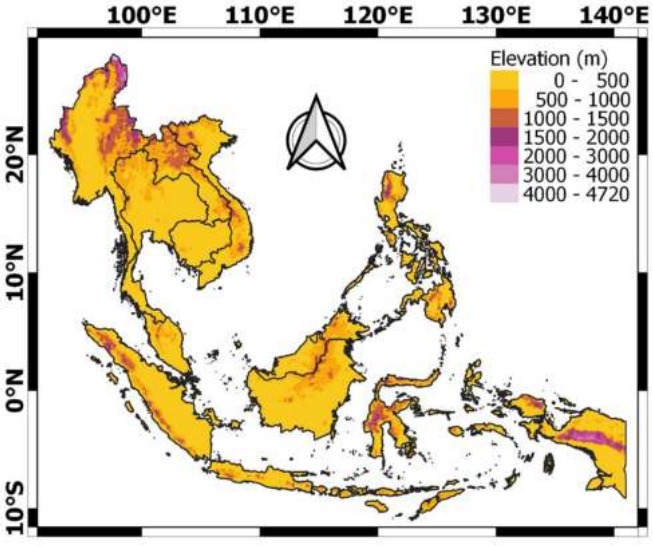

Fig. 1. Southeast Asian topography.

droughts and floods are common in most parts of SEA.

2.2. Gridded rainfall and temperature dataset

To assess the ability of the GCMs' to simulate annual rainfall, and maximum and minimum temperatures, ERA5 - a global high-resolution reanalysis dataset, is used. ERA5 is the fifth edition of the Copernicus Climate Change Service's (C3S) atmospheric, oceanic, and land-surface reanalysis product of the European Centre for Medium-Range Weather Forecasts (ECMWF) (Hersbach et al., 2020). This provides data on 240 atmospheric variables for different pressure level settings. ERA5 is generated by combining an enhanced version of the Integrated Forecasting System (IFS) cycle 41r2 with high-quality global observations. This study used the hourly ERA5 dataset of two climatic variables (e.g., rainfall and near-surface temperature) with a 0.25-degree spatial resolution, spanning the period from January 1979 to December 2005. The hourly rainfall is used to estimate the total monthly rainfall, while the highest and lowest diurnal temperatures were used to extract the average maximum and minimum temperatures. SEA is considered a data-scarce region due to the unavailability of high-quality long-term observation data (Li, 2020). The evenly spaced gridded dataset is generally used for model validation in data-scarce regions. ERA5 is a reanalysis climate data product that provides consistent high-resolution hourly data of several climate variables. It should be noted that several studies have reported the use of ERA5 as a reference dataset near SEA (Khadka et al., 2021; Zhai et al., 2020; Zuluaga et al., 2021).

The spatial distribution of mean annual rainfall, T_{mx} and T_{mn} over SEA is shown in Fig. 2. Hkakabo Razi Mountains in the north and Papua in the south experience the highest annual rainfall (>5000 mm), while the lowest can be found in the middle of Myanmar. T_{mx} is homogeneous in SEA except for the high mountainous regions. T_{mn} ranges from 15 to 30 °C over SEA. However, T_{mn} in the northern region of SEA can be a low as −5 °C.

SEA is subject to a wide variability in climatic conditions. The region is classified into six climate zones based on Köppen climate classification (Peel et al., 2007): tropical rainforest climate (Af), tropical monsoon climate (Am), tropical Savannah climate (Aw), temperate without dry season (Cf), temperature dry summer (Cs), and temperature dry winter (Cw). Due to small areal coverage of Cf, Cs, and Cw, they are combined and included in zone C (Fig. 3). Af is major climate zone over the SEA, covering 47% of total area, whereby annual rainfall varies from 2000 to 4000 mm. During winter, the temperature drops to near freezing point (−5 to 0 °C), particularly in zone C, however it often rises to above 35 °C during some summer days, particularly in Thailand in the Aw zone. Annual rainfall ranges from 760 to 1000 mm in most of the Aw zone. In general, the temperature in both Af and Am zones is greater than 18 °C, however the total rainfall amounts received are different (Alvares et al., 2013).

2.3. Global climate models (GCMs)

This study assesses the performance of 13 CMIP5 GCM's (Taylor et al., 2012) and their updated versions, CMIP6 (Eyring et al., 2016) over SEA. The output of the models have been downloaded from the open-access platform https://esgf-node.llnl.gov. This site provides historical and future projections of monthly rainfall, Tmx and Tmn. The models details are presented in Table 1. Out of several variant labels available, the first one, r1i1p1 for CMIP5 and r1i1p1f1 for CMIP6, is chosen to simplify the evaluation process. CMIP5 investigates several greenhouse gas emissions scenarios through the radiative concentration pathways (RCPs). In CMIP6, new SSPs are used which consider possible changes in the Earth's environment, as well as global economic and demographic trends. Future projections of the RCP 4.5 and 8.5 of CMIP5 are compared with their equivalent radative forcing in CMIP6, SSP2–4.5 and SSP5–8.5 in this study.

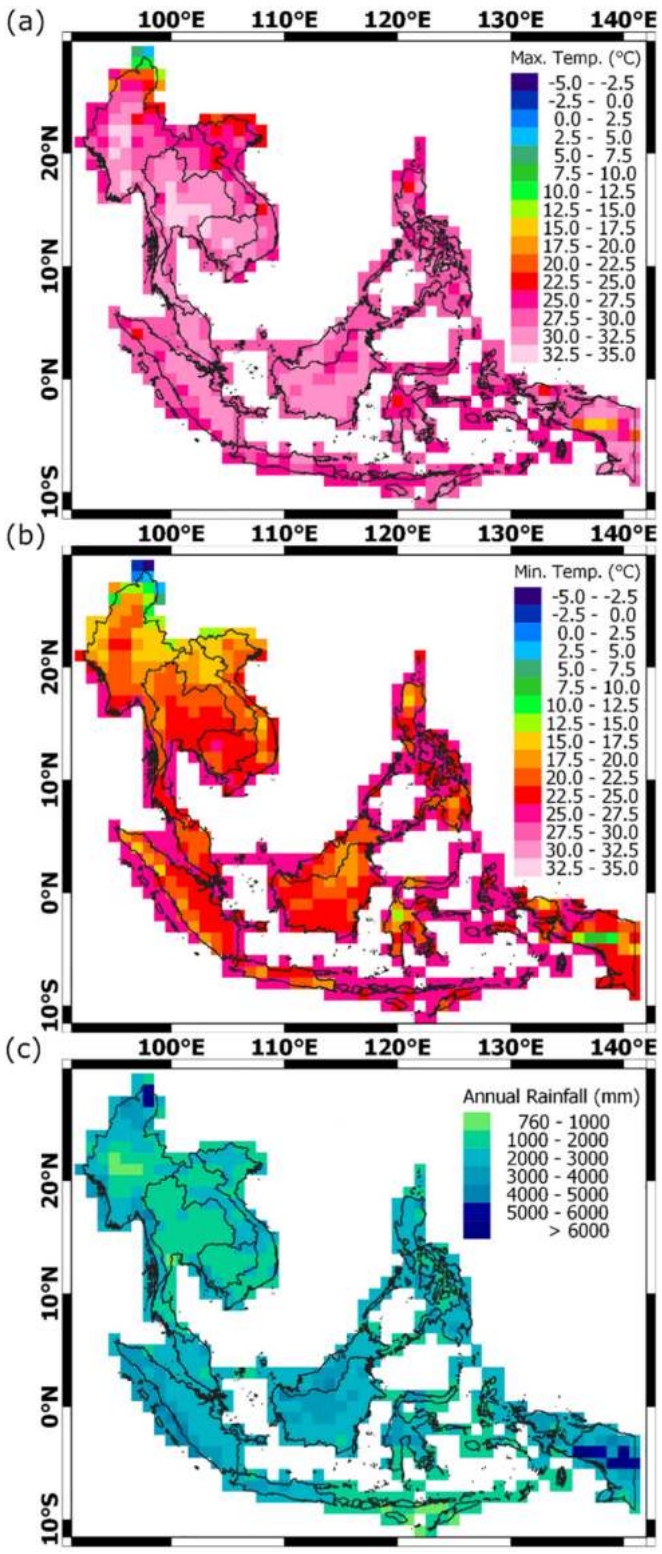

Fig. 2. Spatial variability of yearly mean (a) T_{mx} and (b) T_{mn}, and (c) annual total rainfall over SEA during 1979–2005, estimated via ERA5. (For interpretation of the references to colour in this figure legend, the reader is referred to the web version of this article.)

3. Methodology

ERA5 0.25° × 0.25° reanalysis dataset is used as a reference to evaluate CMIP5 and CMIP6 GCMs. The evaluation process entails

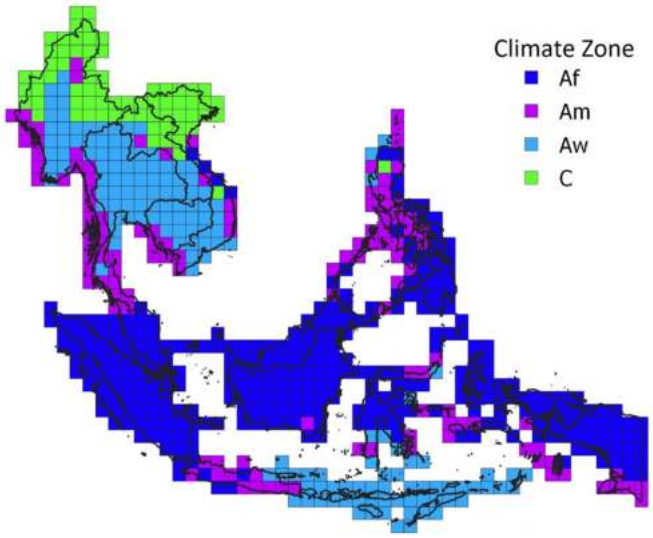

Fig. 3. Köppen climate classification of SEA based on ERA5 (1979–2005). Köppen climate classes are Tropical rainforest climate (Af), Tropical monsoon climate (Am), Tropical Savannah climate (Aw), Temperate without dry season (Cf), Temperature dry summer (Cs), and Temperature dry winter (Cw). (For interpretation of the references to colour in this figure legend, the reader is referred to the web version of this article.)

examining past performance of the three climatic variables (e.g., mean annual rainfall, T_{mx} and T_{mn}). This is carried out using statistical and graphical metrics. Ultimately the model ensemble mean is used to project future changes for each climate zone of SEA for different CMIPs. GCMs have spatial resolution ranges from 0.70° to 3.70° (Table 1), so they are normally interpolated to a common spatial resolution of 1.0° × 1.0° using bilinear interpolation technique. The ERA5 data is also aggregated to the resolution of 1.0° × 1.0°, so all datasets have similar grid sizes and therefore provide an unbiased comparison. Methodological details are presented below.

3.1. Statistical and graphical analyses

The Kling-Gupta efficiency (KGE) is employed to estimate the relative performance of the two CMIPs (Gupta et al., 2009; Kling et al., 2012). The KGE is a single metric designed to evaluate three statistical characteristics together (e.g., Pearson's correlation (r), spatial variability ratio and the normalized variance) as shown in eq. (1). The combination of three metrics provides valuable diagnostic information about the model's performance. KGE is less susceptible to extremes and has greater capability to describe and quantify the overall fitness of GCMs (Radcliffe and Mukundan, 2017). The KGE value varies between 1 and -∞, where 1 represents a complete match. There is no specific meaning attached to the KGE value when it equals zero. However, Knoben et al. (2019) compared the KGE with the Nash-Sutcliff efficiency index and noted that KGE values above −0.41 represented a reasonable performance, while values closer to 1 generally indicated high performance. The KGE is calculated for three climate variables of each GCM compared to the reference dataset (1979–2005).

$$KGE = 1 - \sqrt{(r-1)^2 + \left(\frac{\mu_{GCM}}{\mu_{ref}} - 1\right)^2 + \left(\frac{\sigma_{GCM}/\mu_{GCM}}{\sigma_{ref}/\mu_{ref}} - 1\right)^2} \quad (1)$$

where μ_{GCM} and μ_{ref} are the mean, and σ_{GCM} and σ_{ref} are the standard deviation for GCM and ERA5 data, respectively.

The Taylor diagram (Taylor, 2001) is employed to visually represent the performance of each GCM. The diagram is a robust graphical plot that integrates three statistical metrics, degree of correlation (R), centered root-mean-square error (CRMSE) and ratio of spatial standard deviation (SD). CRMSE determines the discrepancies between two CMIPs and the ERA5 observed data. The blue line in the diagram represents constant CRMSD values, with values increasing with distance from the center.

Statistical tests were employed to estimate the similarity between the seasonal variability of CMIPs and ERA5 rainfall, T_{mx} and T_{mn}, following Baker and Huang (2014). The tests include 1) *t*-test to show the similarity in the mean, 2) F-test to assess the similarity in data variance, and

Table 1
Detailed description of the CMIP5 and CMIP6 GCMs used in this research.

Institution/Country	Abbreviation		Model	Resolution
Australian Research Council Centre of Excellence for Climate System Science, Australia	ACCESS	CMIP 5	ACCESS1–3	1.90 × 1.20°
		CMIP 6	ACCESS-CM2	1.87 × 1.25°
Beijing Climate Center, Beijing, China	BCC	CMIP 5	BCC-CSM1.1-M	2.80 × 2.80°
		CMIP 6	BCC-CSM2-MR	1.12 × 1.12°
Canadian Centre for Climate Modelling and Analysis, Victoria, Canada	CANESM	CMIP 5	CANESM2	2.80 × 2.80°
		CMIP 6	CanESM5	2.79 × 2.81°
Euro-Mediterranean Centre on Climate Change coupled climate model, Italy	CMCC	CMIP 5	CMCC-CM	0.70 × 0.70°
		CMIP 6	CMCC-ESM2	0.94 × 1.25°
EC-Earth Consortium, Europe	EC-EARTH	CMIP 5	EC-EARTH	1.10 × 1.10°
		CMIP 6	EC-Earth3	0.35 × 0.35°
Chinese Academy of Sciences Flexible Global Ocean-Atmosphere–Land System model, China	FGOALS	CMIP 5	FGOALS-g2	2.80 × 2.08°
		CMIP 6	FGOALS-g3	2.00 × 2.00°
Geophysical Fluid Dynamics Laboratory, NJ, USA	GFDL-ESM	CMIP 5	GFDL-ESM2G	2.50 × 2.00°
		CMIP 6	GFDL-ESM4	1.00 × 1.25°
Institute for Numerical Mathematics, Russia	INMCM	CMIP 5	INMCM4.0	2.00 × 1.50°
		CMIP 6	INM-CM5–0	2.00 × 1.50°
Institute Pierre Simon Laplace (IPSL), Paris, France	IPSL-CM-LR	CMIP 5	IPSL-CM5A-LR	3.70 × 1.90°
		CMIP 6	IPSL-CM6A-LR	2.50 × 1.27°
Japan Agency for Marine-Earth Science and Technology (JAMSTEC), Kanagawa, Japan	MIROC	CMIP 5	MIROC5	1.40 × 1.40°
		CMIP 6	MIROC6	1.40 × 1.40°
Max Planck Institute for Meteorology (MPI-M), Germany	MPI-ESM-HR	CMIP 5	MPI-ESM-MR	1.90 × 1.90°
		CMIP 6	MPI-ESM1–2-HR	0.94 × 0.94°
	MPI-ESM-LR	CMIP 5	MPI-ESM-LR	1.90 × 1.90°
		CMIP 6	MPI-ESM1–2-LR	1.87 × 1.86°
Meteorological Research Institute, Ibaraki, Japan	MRI	CMIP 5	MRI-CGCM3	1.10 × 1.10°
		CMIP 6	MRI-ESM2–0	1.12 × 1.12°

3) Kolmogorov–Smirnov (KS) test to evaluate the similarity in data distribution (Sardeshmukh et al., 2000).

3.2. Future projections

Future projections of annual rainfall, T_{mx} and T_{mn} using GCMs of two CMIPs are compared with the historical period (1979–2005) to evaluate possible future climate changes in SEA. Two projections are considered: the medium (RCP4.5 and SSP2–4.5) and high (RCP8.5 and SSP5–8.5) impact scenarios. For a detailed comparison, future horizon was divided into near (2020–2059) and far (2060–2099) futures. The median and 95% confidence band of the projection interval are considered for each scenario in order to quantify the associated uncertainty of the different CMIP models. The seasonal variability of different climate zones for rainfall, T_{mx} and T_{mn} are measured for each model. Finally, maps are prepared to depict percentage of change in rainfall and absolute change in temperatures (°C).

4. Results

4.1. Evaluating skills of CMIP5 and CMIP6 GCMs

Fig. 4 depicts the ability of two CMIPs to replicate annual rainfall, T_{mx}, and T_{mn} in terms of KGE. A single radar chart is used to present KGE of CMIP5 (in light green) and CMIP6 (in light red) GCMs for each climate variable. KGE values less than zero on the rainfall radar chart are defined as zero for illustration purposes. It shows that GCMs are able to estimate T_{mn} better than T_{mx} and rainfall in SEA. The performance of the CMIP5 models and their improvements in CMIP6 are almost the same in simulating T_{mx} and T_{mn}. Few models of CMIP6 simulated T_{mx} better than previous versions, namely: MPI-ESM-HR, IPSL-CM-LR, GFDL-ESM, EC-Earth, CanESM and MRI. Both versions of FGOALS simulated a lower value of T_{mx} than other models, indicating poor modelling capability. For T_{mn}, only five models of CMIP6 indicated better performance than their predecessors, including MPI-ESM-HR, INM-CM, GFDL-ESM, EC-Earth and CanESM. INM-CM showed the largest improvement in CMIP6 for T_{mn}. Although the performance of the models of both CMIPs was nearly identical in replicating historical temperatures, CMIP6 GCMs displayed an enhanced ability to simulate historical rainfall in all cases apart from FGOALS and IPSL-CM-LR. Among the CMIP6 models, EC-EARTH was best in replicating all variables. ACCESS of CMIP6 exhibited the best performance in replicating rainfall (KGE 0.59) and CMCC of CMIP5 in replicating T_{mx} and T_{mn} (KGEs 0.86 and 0.92, respectively). KGEs of both FGOALS and IPSL-CM-LR were poor (KGEs −0.31 and −0.48, respectively) for rainfall, therefore indicating poor capability.

KGE is the integration of three statistical metrics, namely Pearson's correlation (r), mean of GCM to mean of ERA5 (β) and variability ratio (γ). Fig. 5 presents the three components of KGE in terms of r, β-1 and γ-1 aiming to illustrate the most influencer component of the final KGE score. The r, β, γ and KGE of CMIP5 and CMIP6 GCMs in simulating historical rainfall are presented in blue and red bars. The result indicates that all the components contribute significantly to a higher value of KGE. However, models that have near optimum values of β and γ (e.g., MPI-ESM-LR) showed a low KGE due to low r, indicating a bit higher influence of spatial correlation on model performance.

4.2. Taylor diagram

The ability of the two CMIP models to estimate annual rainfall, T_{mx} and T_{mn} are presented (along with their MME means) as Taylor diagrams (Fig. 6). Hollow circle on the x-axis presents reference data (i.e., ERA5). The CMIP5 and CMIP6 models are represented using coloured circles and triangles, respectively. The model symbol nearest to the hollow circle indicates the best performing model. The correlation of the models with the reference data is best for T_{mn} (0.85). This is followed by T_{mx} (0.75) and then rainfall (0.45). A strong correlation for T_{mn} indicates better capability of GCMs of both CMIPs in modelling T_{mn}. Model over and underestimation, however, is noted. FGOALS of both CMIPs underestimated T_{mx} and T_{mn} variability, while INM-CM5–0 overestimated T_{mn} variability. The majority of models, of both CMIPs, simulated observed rainfall variability reasonably well, except for a large overestimation by IPSL-CM6A-LR and FGOALS-g3.

4.3. Seasonal variability

The multimodel ensemble (MME) medians of the available 13 GCMs for both CMIPs have been used to show bias in the seasonal variability of temperature and rainfall for each climatic zone when compared to ERA5. Fig. 7 shows the month-to-month bias in T_{mx}. This is estimated by subtracting the CMIPs MME from ERA5. The dashed red line represents the bias in the CMIP5 MME median, while the dashed blue line represents the bias in the CMIP6 MME median. The horizontal black dashed line represents the zero bias. The 95% confidence interval band of GCMs' bias has also been provided to show simulation uncertainty.

Overall, the bias in MME median of CMIP6 was more aligned to the zero line than CMIP5. The 95% confidence interval band of the CMIP6 ensemble was also thinner, suggesting lower uncertainty in their estimates of T_{mx} than for CMIP5. The results also indicated that the inner model differences of CMIP6 were far less than for CMIP5. Both versions of CMIPs displayed higher uncertainties in simulating seasonal variability of T_{mx} in climate zone C than in other zones. Both CMIPs underestimated T_{mx} in zone Af. CMIP6 overestimated T_{mx} in Am for all months, except January and February. Both versions also underestimated T_{mx} in the Aw climate zone for all months, except for the April to June period.

Fig. 8 presents the month-to-month viability of bias in T_{mn}, estimated by the two CMIPs. Like T_{mx}, CMIP5 shows larger inter-modality in T_{mn} than CMIP6. This indicates low uncertainty in the CMIP6 simulations when compared to CMIP5. For most months, a subtle overestimation by GCMs of both CMIPs was noticed for the Af and Am zones, especially by CMIP6. The median bias for the MMEs was nearly identical with ERA5 for the climate zone C, while the bias confidence interval band of CMIP5 was between −11 and 4 °C.

Similar results are seen for rainfall. Uncertainty in the CMIP6 rainfall bias (Fig. 9) band is thinner than CMIP5 bias for all climate zones. However, CMIP6 MME overestimated rainfall for the Af zone to a greater degree than for CMIP5 MME. In the Am and Aw zone, MME of both CMIPs under and overestimated monsoon rainfall, respectively. The differences were greater for CMIP6 MME. The highest underestimation by both CMIP MMEs was noted in zone C. Both CMIPs MME median and confidence interval band were below zero for most of the months. This indicates an underestimation of rainfall by all GCMs for both CMIPs in this zone.

Overall, the results support the findings determined in statistical evaluations of the models. Table 2 presents the results of the *t*-test, KS test and F-test for seasonal rainfall, T_{mx} and T_{mn} of CMIPs seasonal median and ERA5 in different climate zones. Both CMIP5 and CMIP6 seasonal MME were statistically indistinguishable at the 95% level based on all three tests in all climate zones, except zone Af for the t-test and KS test. The results indicate no significant difference in CMIP5 and CMIP6 models in SEA. Inter-model variability of CMIP6 GCMs, however, was less than for the CMIP5 GCMs. The uncertainty in simulations in CMIP6, therefore, was lower than for the CMIP5 GCMs.

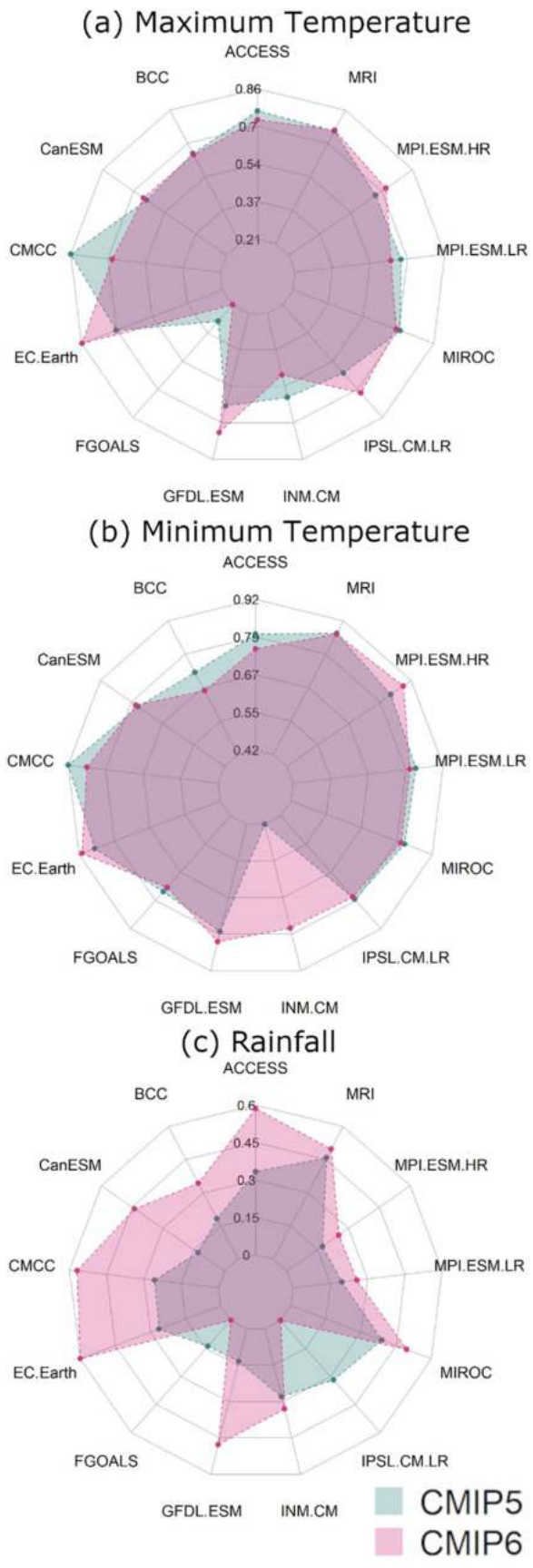

Fig. 4. Performance of CMIP5 and CMIP6 GCMs in estimating historical annual average: (a) T_{mx}, (b) T_{mn}; and (c) rainfall during 1979–2005. (For interpretation of the references to colour in this figure legend, the reader is referred to the web version of this article.)

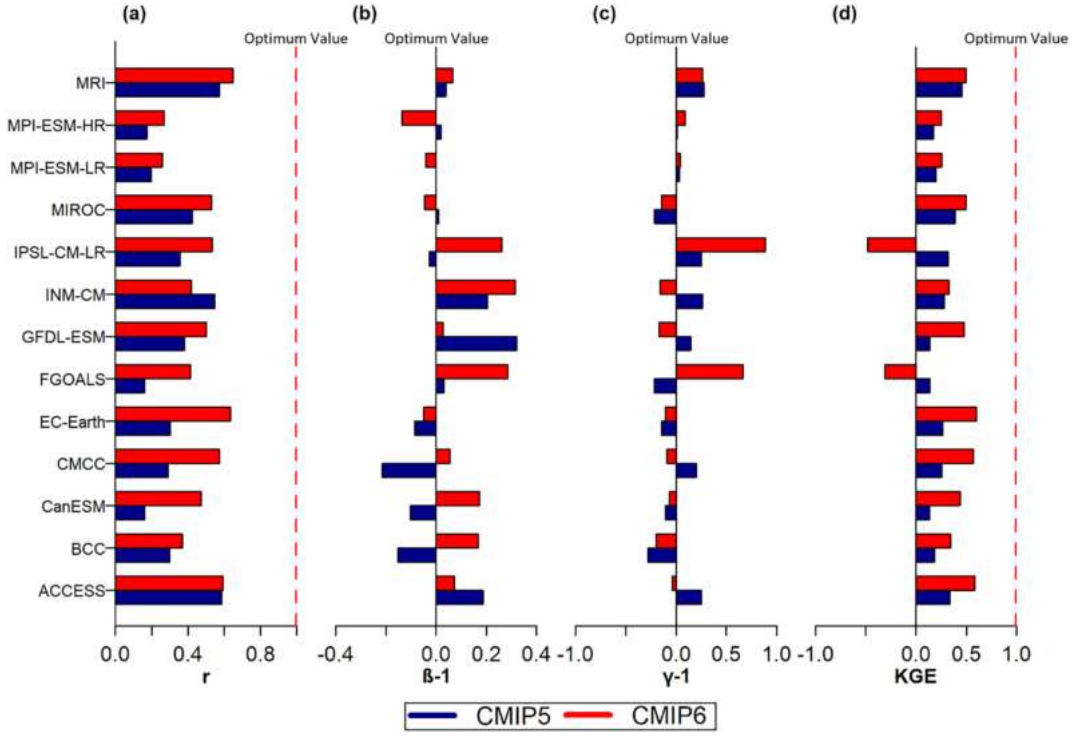

Fig. 5. Bar charts show the performance of CMIP5 and CMIP6 in simulating historical rainfall based on KGE and its components. (For interpretation of the references to colour in this figure legend, the reader is referred to the web version of this article.)

4.4. Projected T_{mx}, T_{mn} and rainfall

Fig. 10 shows the temporal evolution of T_{mx} (plots a and b) and T_{mn} (plots c and d) averaged over SEA by the MMEs of CMIP5 and CMIP6 for differing scenarios. The upper plots (e.g., a and c) show the projection for medium emission scenarios; RCP4.5 for CMIP5 and SSP2–4.5 for CMIP6, respectively, while the lower plots (e.g., b and d) show the projection for high-end scenarios; RCP8.5 for CMIP5 and SSP5–8.5 for CMIP6, respectively (Fig. 10). The MME median projection is presented using an intermediate solid line for the applicable historical period (1979–2005 for CMIP5 and 1979–2014 for CMIP6) and the dashed line for the future period, while the band presents the 95% confidence interval of the projections. The blue line represents CMIP6, and the brown line represents CMIP5. A 30-year moving average is used to smooth the lines.

Fig. 10 shows a much thinner confidence band (less uncertainty) in the projections for CMIP6 than its predecessors, CMIP5. For T_{mx}, both versions show nearly the same future projection for different scenarios for 2020–2059. CMIP6 shows a greater increase in T_{mx} for SSP2–4.5 and a reduced increase for SSP5–8.5 compared to RCP4.5 and 8.5 projections for 2060–2099. T_{mx} is projected to reach 30.2 °C and 31.74 °C for SSP2–4.5 and 5–8.5, while 29.9 °C and 31.97 °C for RCP4.5 and 8.5 by 2100. The CMIP5 MME median shows an abrupt shift in T_{mx} between the historical estimations and the modelling forecasts. This is not seen in the CMIP6 modelling. A gradual increase in T_{mx} from historical to future periods indicates a realistic projection by CMIP6.

The MME median of CMIP6 shows a slight decrease in T_{mn} in the future (when compared to the CMIP5) for both scenarios (Fig. 10). The T_{mn} is projected to reach 25.11 °C and 26.6 °C for SSP2–4.5 and 5–8.5, and 25.29 °C and 26.7 °C for RCP4.5 and 8.5 by 2100. As is the case for T_{mx}, CMIP6 also shows reduced uncertainty in the T_{mn} projection when compared to CMIP5.

Fig. 11 shows rainfall projections generated by CMIP5 and CMIP6 MME. The MME median of CMIP6 indicates the potential for a greater increase in rainfall in the future than does CMIP5. The uncertainty in the projections of both CMIPs, however, is similar. The CMIP6 MME projected an increase in rainfall from nearly 2500 mm from the present day to 2700 mm by 2100 for SSP2–4.5, while CMIP5 MME indicated a potential for 2577 mm for RCP4.5 (Fig. 11 (a)). For the higher scenario, the MME of both CMIPs projected the rainfall to reach 2640 mm by 2100 (Fig. 11 (b)). Results indicate a greater decrease in rainfall for SSP5–8.5 than for SSP2–4.5, and a greater increase in rainfall for RCP8.5 than RCP4.5.

4.5. Spatial changes of temperature and rainfall

Changes in annual T_{mx}, T_{mn} and rainfall were estimated using the MME mean of CMIPs for both the near and far futures, and for both the medium and high scenarios. These were compared to the historical period (1979–2005).

Fig. 12 depicts the geographical distribution of projected change (°C) in T_{mx}. Both CMIPs projected a rise in T_{mx} for the two future periods. However, CMIP6 MME projected a smaller rise in T_{mx} than did CMIP5 MME. The projections of both CMIPs are highly consistent. Both MMEs projected a maximum increase in T_{mx} in the north (> 4.0 °C), and a minimum to the southeast (Papua), with a temperature of 1.0–1.33 °C in the near future and 1.59–3.01 °C in far future. T_{mx} projections also show a reduced rate of temperature increase in the central parts of SEA.

The increase in T_{mn} was similar to T_{mx} (Fig. 13). In contrast to T_{mx}, however, the CMIP6 MME modelling projected a greater increase in T_{mn} than for CMIP5 MME, for both projection scenarios in both periods. Overall, T_{mn} is projected to increase more than T_{mx}. The greatest

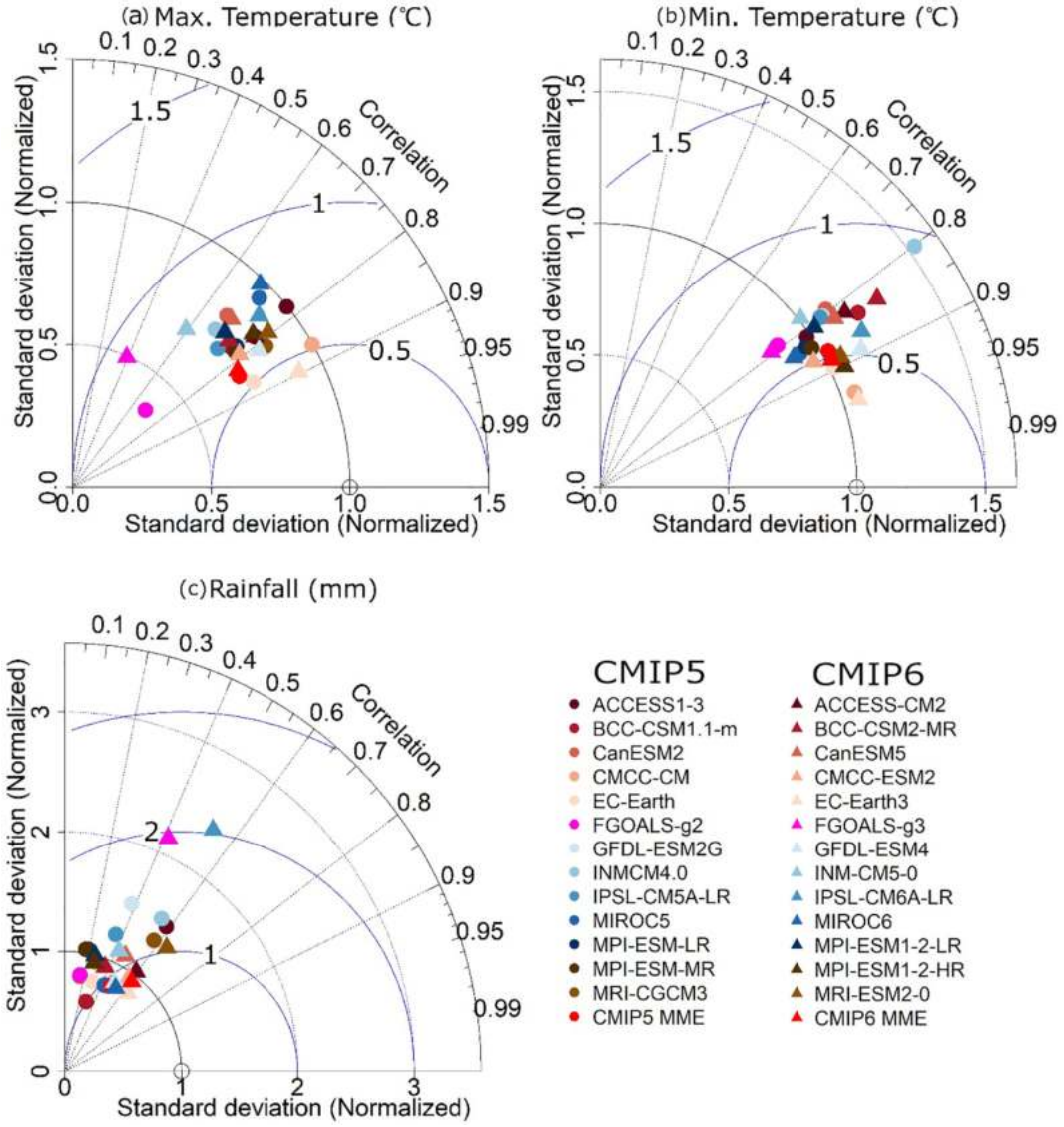

Fig. 6. Taylor diagrams, showing skill of the GCMs of two CMIPs in simulating: (a) T_{mx}; (b) T_{mn}; and (c) rainfall. (For interpretation of the references to colour in this figure legend, the reader is referred to the web version of this article.)

increase is seen in the north (5.02 °C), while the lowest is in the southeast, 0.96–1.27 °C in near future and 1.57–3.08 °C in far future. Both T_{mn} and T_{mx} show the greatest increase in regions where historical temperatures are less and vice versa.

Fig. 14 shows the geographical variability in the projected changes in annual rainfall in percent. Both the CMIPs MME provided projections for annual rainfall for both the medium and high scenarios. The greatest increase is projected for the near future for SSP2–4.5. Both CMIPs, however, display a 25% decrease in rainfall in the south (Java) and southwest (Sumatra) parts of SEA. Rainfall increases in the northwest (Borneo and Indonesia) and the southeast (Papua). A 10 to 20% increase in rainfall in those regions is projected in the far future, for all scenarios. Rainfall would increase in the higher rainfall regions of SEA.

5. Discussion

A large number of studies have examined the ability of CMIP5 and CMIP6 GCMs to estimate the historical climate in different regions of the globe (Jain et al., 2019; Gusain et al., 2020; Kamruzzaman et al., 2021; Song et al., 2021a; Yazdandoost et al., 2021). Overall, these studies have revealed an improvement in the CMIP6 models compared to previous versions, i.e. CMIP5. Improvements in CMIP6 modelling have been noted in studies of the Tibetian Plateau (Lun et al., 2021), Central and South America (Ortega et al., 2021), Columbia (Arias et al., 2021), Meditteranean region (Bağçaci et al., 2021). The superiority of CMIP6 models over the older CMIP5 models was also reported for extreme indices work over East Africa (Ayugi et al., 2021), extreme rainfall and temperature in major river basins of China (Zhu et al., 2021), extreme precipitation over the whole of China (Luo et al., 2021), Australia (Deng et al., 2021), and Western North Pacific and East Asia (Chen et al., 2021). CMIP6 models were found to simulate climatic variables more accurately than CMIP5 models. For example, Jiang et al. (2021) found improved measurement of clouds and vapor over the tropical ocean using CMIP6. In the nearby region of SEA, Jain et al. (2019) reported enhancement of CMIP6 GCMs over Central and North India. Gusain et al. (2020) reported the higher capability of CMIP6 GCMs in estimating the

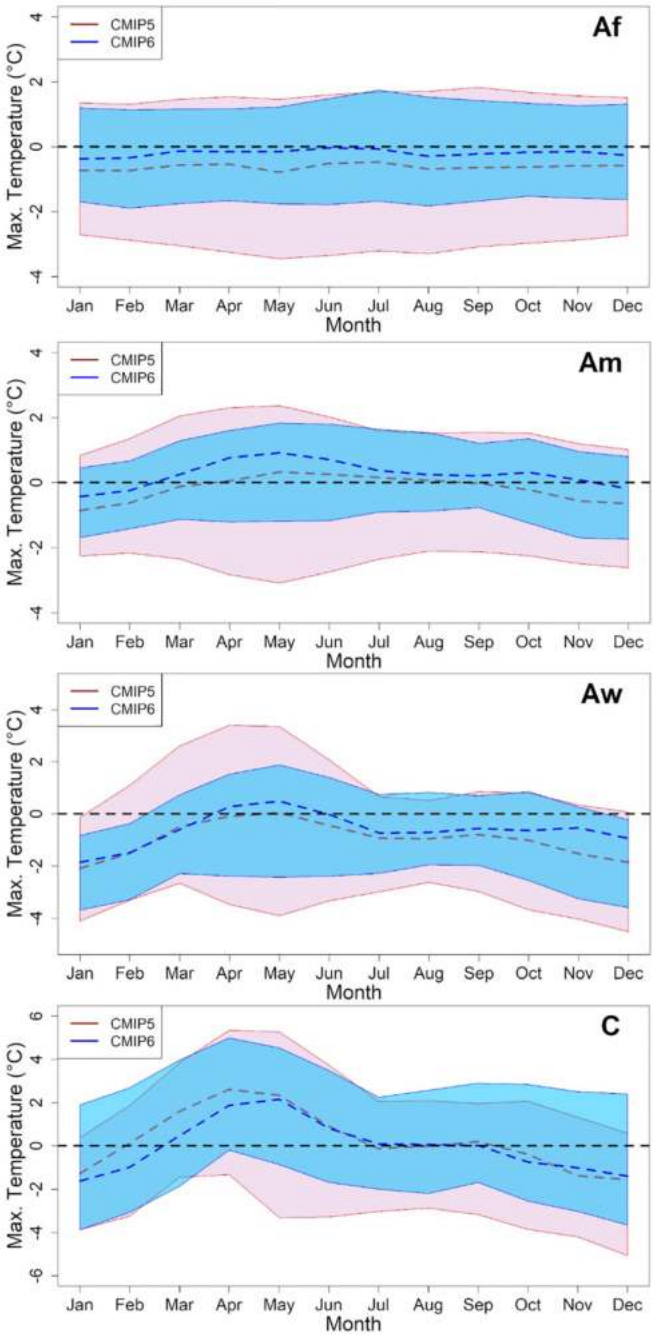

Fig. 7. Seasonal variability in mean bias in Tmx of CMIP5 and CMIP6 GCMs compared to ERA5 dataset for four different climate zones (AF, Am, Aw and C) of SEA. (For interpretation of the references to colour in this figure legend, the reader is referred to the web version of this article.)

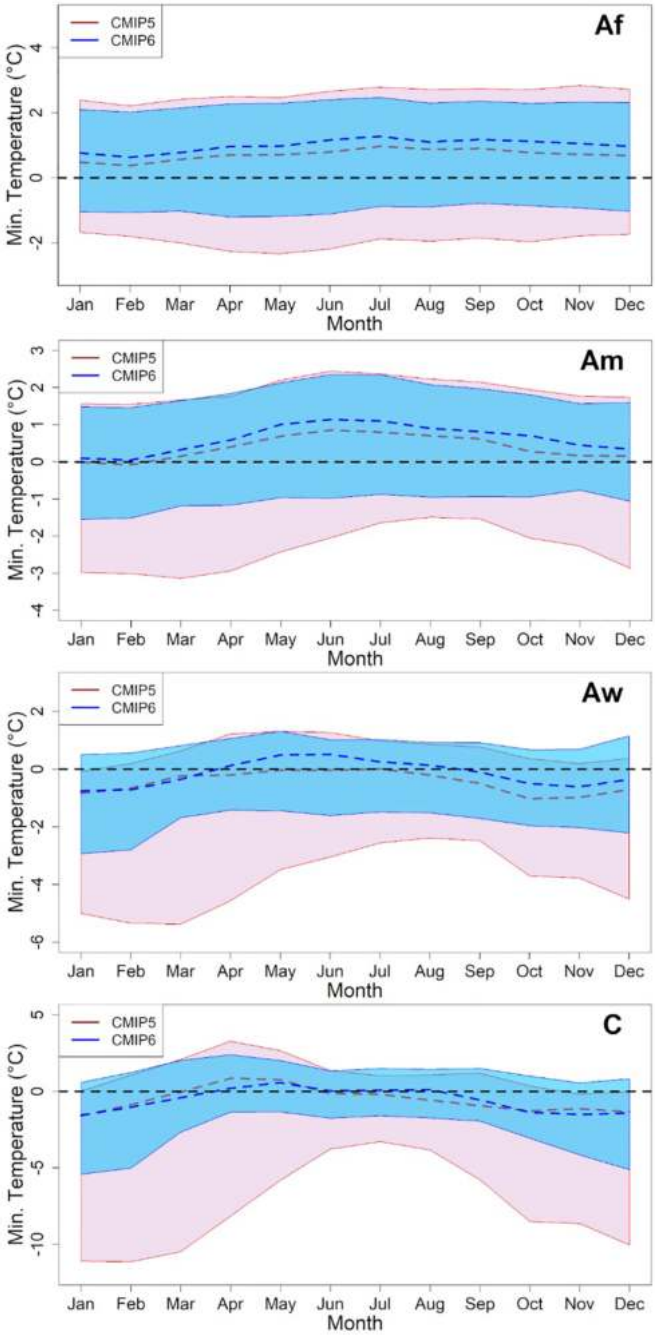

Fig. 8. Same as Fig. 7, but for Tmn. (For interpretation of the references to colour in this figure legend, the reader is referred to the web version of this article.)

Indian summer rainfall. Song et al. (2021b) showed an improvement in CMIP6 modelling over South Korea. Kamruzzaman et al. (2021) found there was an enhanced ability of CMIP6 MME to replicate spatial variability of rainfall and temperature over Bangladesh when compared with CMIP5 MME.

The current study findings were different to those noted in other parts of the world, with the performance of CMIP6 GCMs found to be similar to that of CMIP5. The KGE showed an improvement in some of the CMIP6 GCMs in simulating historical rainfall, however, the Taylor diagram indicated similar performance of GCMs for both CMIPs. The major difference in the CMIP6 models when compared to the CMIP5 models was less inter-model variability. Due to this, the uncertainty bond in CMIP6 ensemble was much narrower than in the CMIP5 ensemble. A comparable finding is reported by Deng et al. (2021) when comparing the performance of CMIPs in simulating temperature extremes over Australia. These showed narrower ensemble ranges for CMIP6 models when compared to CMIP5 models (Deng et al., 2021). These results indicate more consistency in simulations using CMIP6 GCMs when compared to CMIP5 GCMs. All CMIP6 GCMs used the same forcing datasets and boundary conditions (Taylor et al., 2018). Therefore, the simulations of CMIP6 GCMs are more consistent.

The results reported here also contradict the findings from Khadka et al. (2021) over SEA. That study did not use common models to compare both CMIPs and also used different subsets of the CMIP5 and CMIP6 GCMs. In the current study, common GCMs for both CMIPs were

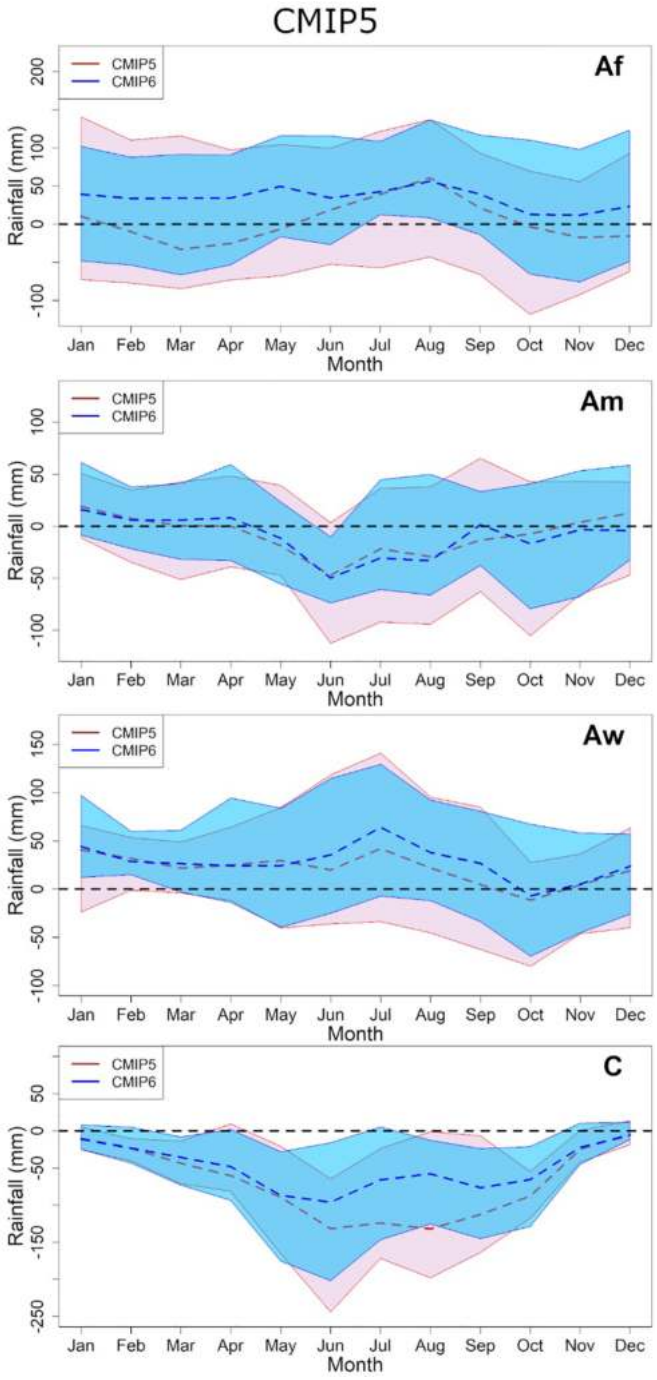

Fig. 9. Same as Fig. 7, but for rainfall. (For interpretation of the references to colour in this figure legend, the reader is referred to the web version of this article.)

Table 2
The results obtained using Student's t-test, KS and F-test for historical seasonal T_{mx}, T_{mn} and rainfall of CMIP5 and CMIP6 against ERA5 in different climate zones. Zero (0) indicates that the test supports the null hypothesis of no difference, while one (1) indicates rejection of the null hypothesis at the 5% significance level.

Variable	Month	Zone Af			Zone Am			Zone Aw			Zone C		
		t	KS	F	t	KS	F	t	KS	F	t	KS	F
Tmx	CMIP5 vs ERA5	1	1	0	0	0	0	0	1	0	0	0	0
	CMIP6 vs ERA5	0	0	0	0	0	0	0	1	0	0	0	0
Tmn	CMIP5 vs ERA5	1	1	0	0	0	0	0	0	0	0	0	0
	CMIP6 vs ERA5	1	1	0	0	0	0	0	0	0	0	0	0
Rainfall	CMIP5 vs ERA5	0	0	0	0	0	0	0	0	0	0	0	0
	CMIP6 vs ERA5	1	0	0	0	0	0	0	0	0	0	0	0

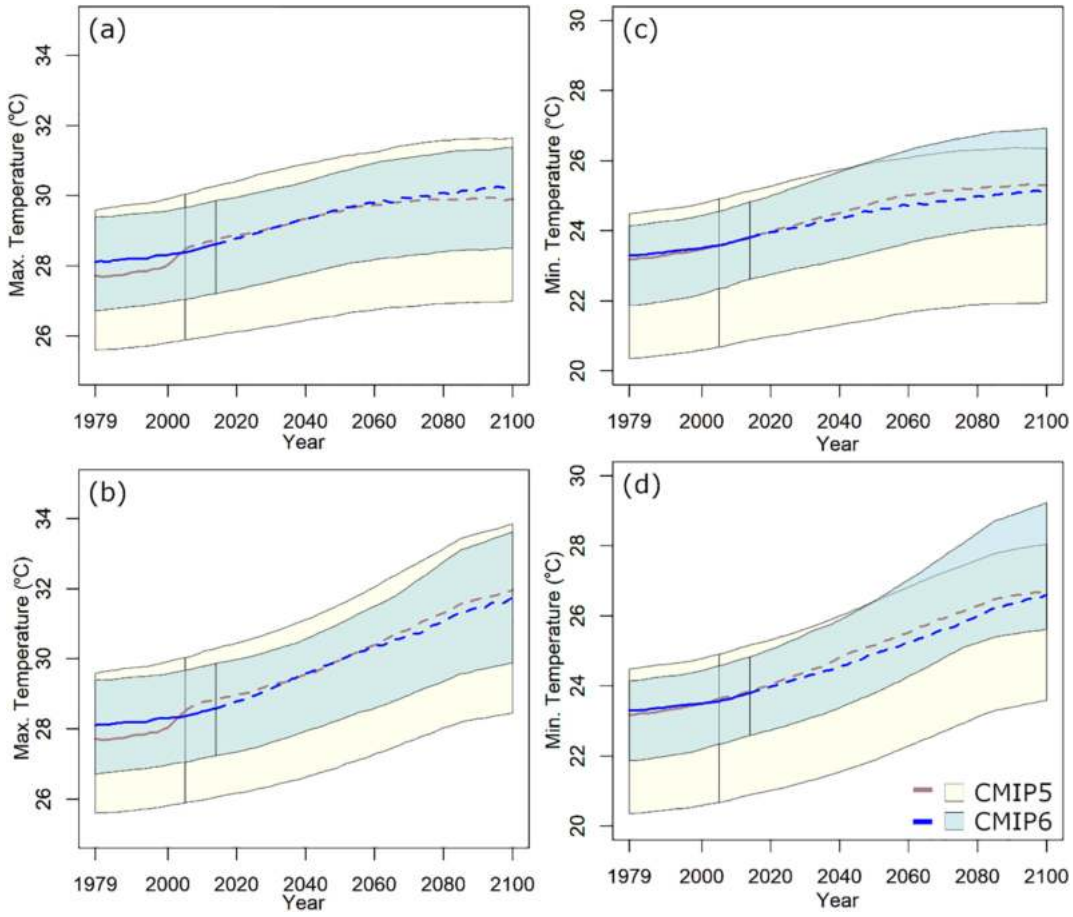

Fig. 10. Temporal evolution of T_{mx} (°C) (a and b) and T_{mn} (°C) (c and d) for CMIP5 (yellow) and CMIP6 (blue) under different scenarios (upper row) RCP4.5 and SSP2–4.5 and (lower row) RCP8.5 and SSP5–8.5. Shadings signify 95% projections confidence interval. The vertical line indicates the end of the historical estimations. (For interpretation of the references to colour in this figure legend, the reader is referred to the web version of this article.)

used and so provided an estimation of the relative performance of the GCMs. Khadka et al. (2021) also used correlation and RMSE for measuring the performance of the GCMs. So two metrics were used to estimate different properties of the model performance. It should be noted that making decisions using multiple statistical metrics is always problematic, as using different metrics can often provide different outcomes. For this reason, the current study used an integrated metric (KGE). This measures the ability of the model to construct spatial distributions, variables and bias, and thus has provided a reliable assessment of GCM capability.

The SEA is comprised of both mainland and maritime continents. Shallow and deep marginal seas, with complex land-sea distribution and topography, have resulted in a complex climatic regime (Robertson et al., 2011). Atmospheric circulation patterns (resulting from the land-sea configuration) make seasonal temperatures and rainfall asymmetric over the region (Yoneyama and Zhang, 2020). These factors may have influenced CMIP6 modelling performance and affected the improved capability noted in other studies when comparing performance against the older CMIP5 models.

This study reported some inconsistencies in the projection of temperature and rainfall for both the CMIP5 and CMIP6 models. CMIP6 showed a large increase in T_{mx} for SSP2–4.5 and a small increase for SSP5–8.5, compared to RCP4.5 and 8.5, for the far future projections (2060–2099). The MME mean of CMIP6 showed a slight decrease in T_{mn} in future than CMIP5 for both scenarios. In contrast to T_{mx}, CMIP6 MME projected an increase in T_{mn} compared to CMIP5 MME for both projection scenarios in all periods. This has also contradicted the findings available for other regions. SSP scenarios have previously been reported as indicating a greater increase in temperature than their equivalent RCP scenarios (Ortega et al., 2021). However, both CMIPs have reported a greater increase in T_{mn} when compared to T_{mx}, as noted in other regions. The greatest inconsistency in the CMIP5 and CMIP6 GCMs was in the rainfall projections. The results showed a decrease in rainfall for SSP5–8.5 as compared to SSP2–4.5, with an increase in rainfall noted for RCP8.5 compared to RCP4.5. This indicated an increase in rainfall with increase in temperature for CMIP5 MME in the region. In contrast, CMIP6 MME showed a decrease in rainfall for SSP5–8.5 despite a rise in temperature.

The spatial distribution of temperature and rainfall changes revealed a greater increase in temperature in the cooler regions and a reduced increase in the warmer regions. This was in contrast to the rainfall projections. Increased rainfall was noted in the high rainfall regions and reduced rainfall in the current low rainfall regions. The results indicated more homogeneity in the geographical variability of temperature, but more heterogeneity in the spatial distribution of rainfall. The current temperature in the region is more homogeneous than in any other part of the world and the present study indicates that this would continue into the future. In contrast, the current spatial distribution of rainfall in SEA

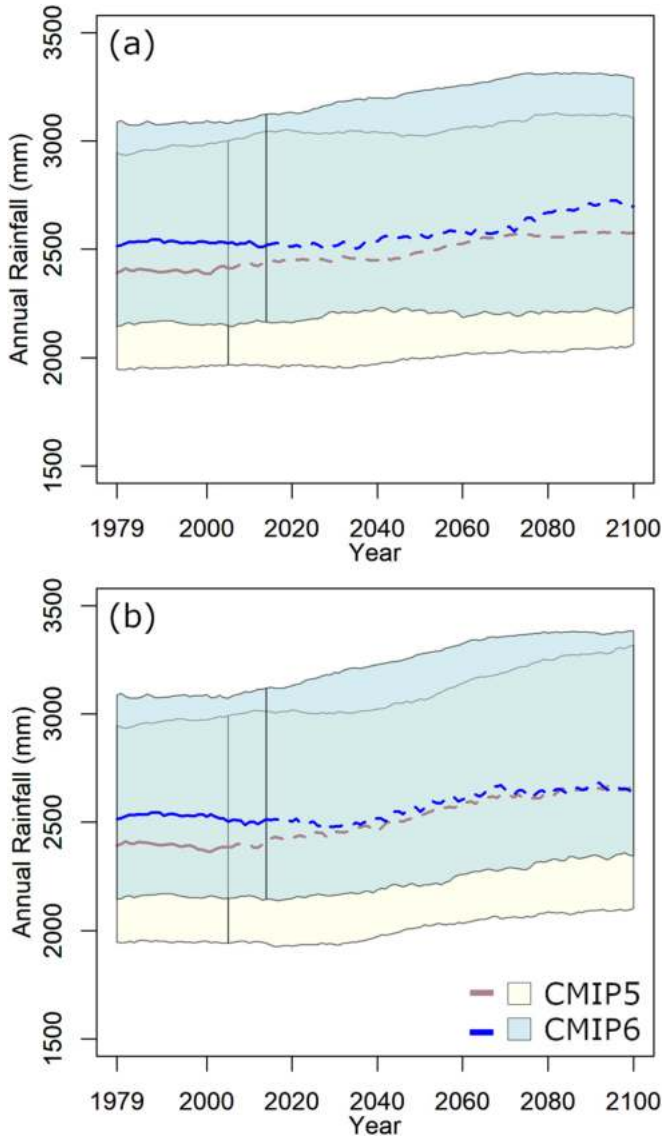

Fig. 11. Annual rainfall (mm) projection by CMIP5 (yellow) and CMIP6 (blue) models for different scenarios: a) medium scenario (RCP4.5 and SSP2–4.5); and b) high scenario (RCP8.5 and SSP5–8.5). (For interpretation of the references to colour in this figure legend, the reader is referred to the web version of this article.)

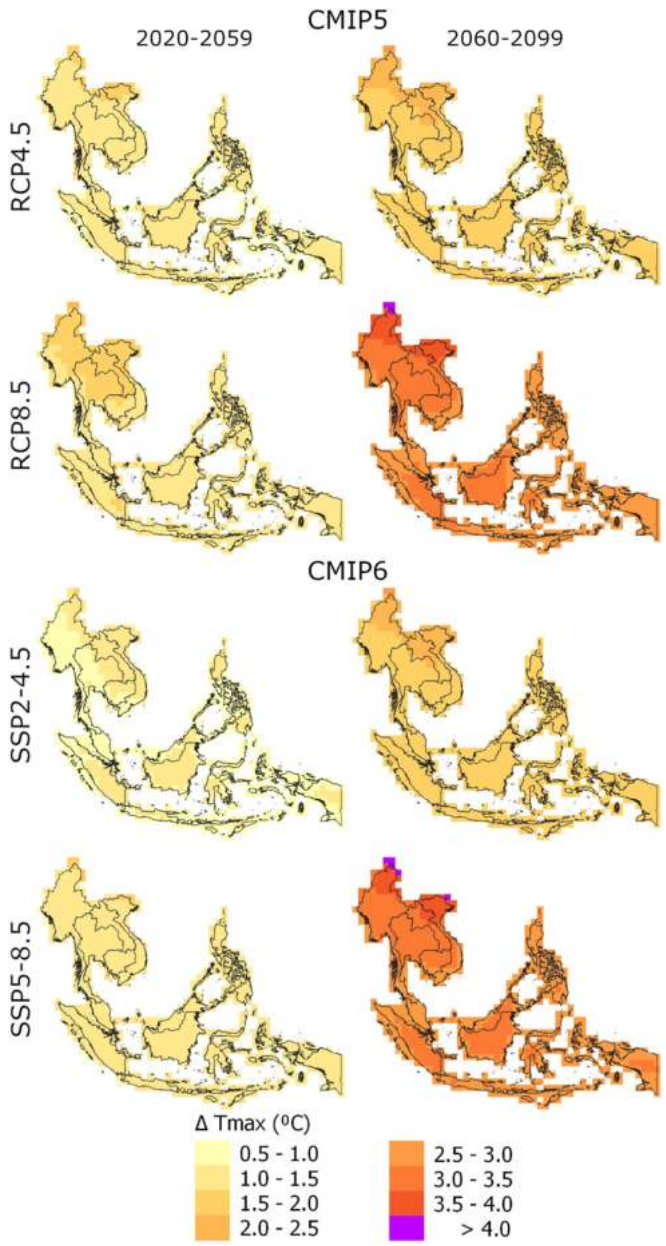

Fig. 12. Geographical variability of the change in T_{mx} (°C) over SEA based on MME of CMIP5 and CMIP6 for two futures in medium and high projection scenarios.

is highly diverse, ranging from 750 mm to >6000 mm. Some parts of Papua in the southeast receive the highest rainfall globally (~ 11,000 mm). The SEA has the highest density of animal life on the planet with the various species inhabiting a narrow climatic niche. Climate change is expected to increase species diversity.

6. Conclusion

The present study evaluated the use of CMIP5 and CMIP6 in developing present and future climate projections for the Southeast Asia region. Uncertainties in historical simulation and future projections of the CMIPs were also examined as part of determining overall model performance. The study revealed no significant improvement in GCMs (from CMIP5 to CMIP6) in simulating present-day temperature and rainfall over SEA. However, the CMIP6 ensemble did display less uncertainty in the simulation work than CMIP5. This indicated a greater degree of confidence could be assumed in any decision-making based on the CMIP6 projections. Both CMIPs revealed that a rise in temperature and rainfall in most of SEA would occur. Some inconsistencies in the CMIP5 and CMIP6 models projections were noted. This has emphasized the need to streamline existing adaptation measures, particularly those arising from CMIP6 SSP scenarios. The study projected a decrease or an insignificant increase in rainfall in the low rainfall region. This may increase both flood and water stress in the region. Any changes in the homogeneity in temperature and rainfall could significantly affect the biodiversity in the region. Future modelling should take account of the increased availability of GCMs both CMIPs, and utilize the ability to compare and contrast the various model iterations.

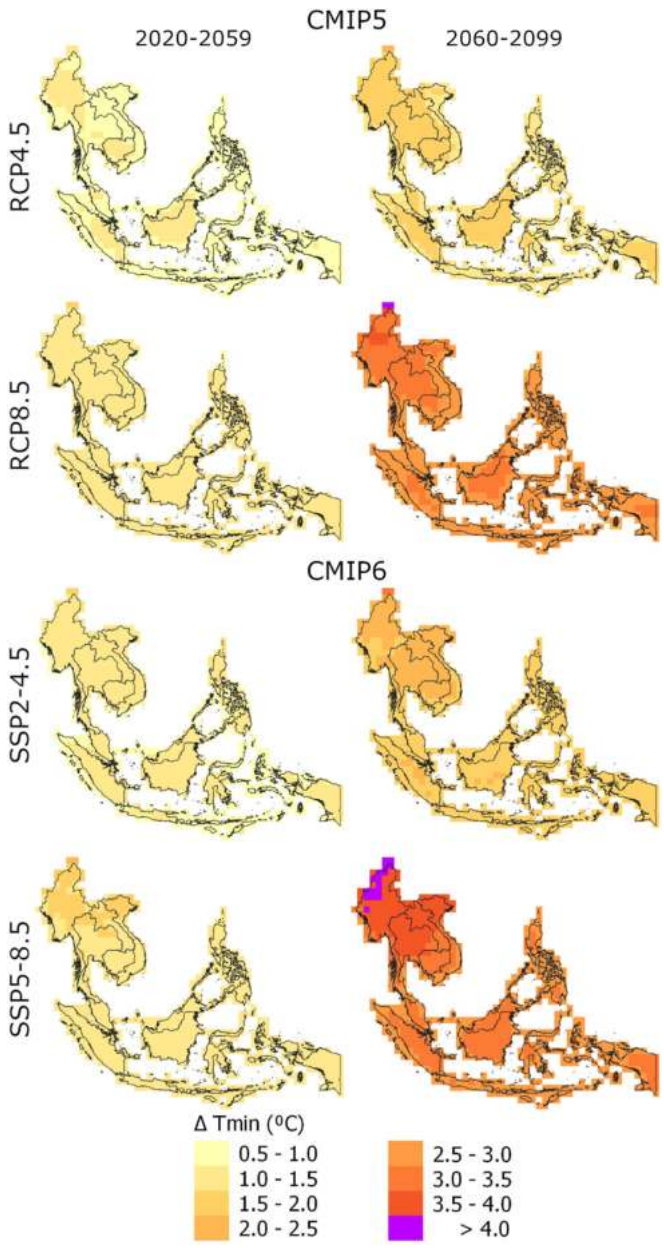

Fig. 13. Same as Fig. 12, but for Tmn (°C).

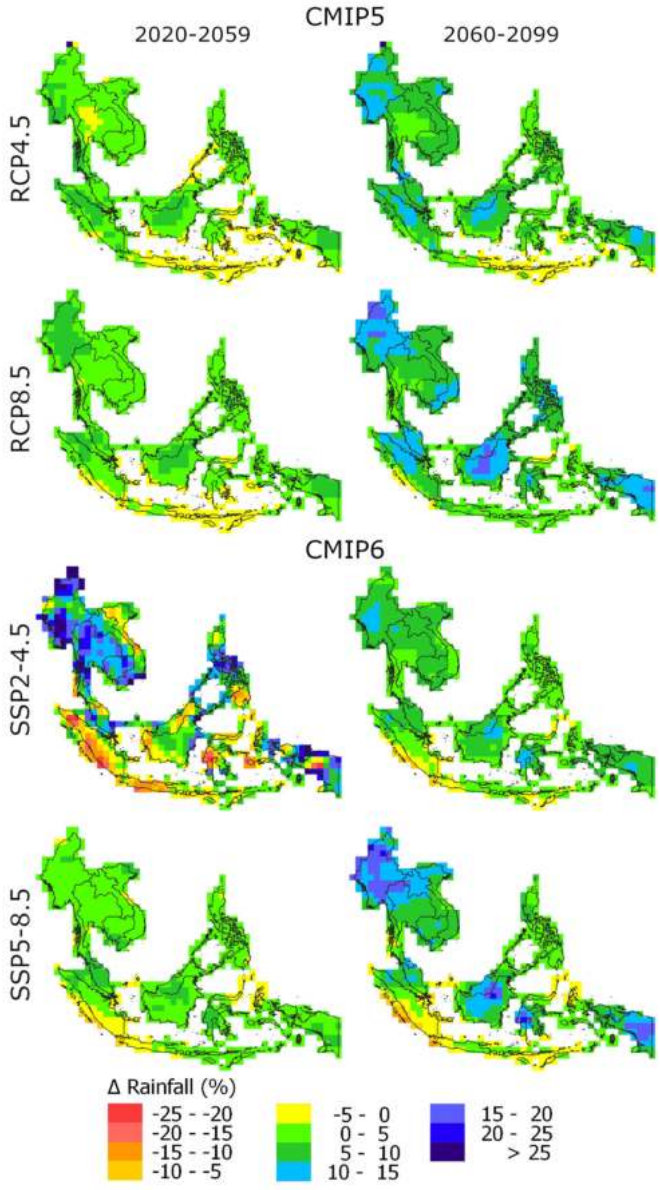

Fig. 14. Same as Fig. 12, but for rainfall.

Funding

The authors are grateful to Staffordshire University, UK for providing financial support for this research through grant no. WR GCRF 2020–2021. Authors are also grateful to the Belt and Road Special Foundation of the State Key Laboratory of Hydrology-Water Resources and Hydraulic Engineering to support this research through grants no. (2019491311 & 2020491011).

Code availability

The code was written using R software, R.3.4, to produce the data. The code is available upon request.

Author contributions

All authors contributed to the study conception and design.

Declaration of Competing Interest

The authors declare that they have no known competing financial interests or personal relationships that could have appeared to influence the work reported in this paper.

References

Alvares, C.A., Stape, J.L., Sentelhas, P.C., De Moraes Gonçalves, J.L., Sparovek, G., 2013. Köppen's climate classification map for Brazil. Meteorol. Z. 22, 711–728. https://doi.org/10.1127/0941-2948/2013/0507.

Arias, P.A., Ortega, G., Villegas, L.D., Martínez, J.A., 2021. Colombian Climatology in CMIP5/CMIP6 Models: Persistent Biases and Improvements. Rev. Fac. Ing. Univ, Antioquia.

Ayugi, B., Jiang, Z., Zhu, H., Ngoma, H., Babaousmail, H., Karim, R., Dike, V., 2021. Comparison of CMIP6 and CMIP5 models in simulating mean and extreme precipitation over East Africa. Int. J. Climatol. https://doi.org/10.1002/joc.7207 n/a.

Bağçaci, S.Ç., Yucel, I., Duzenli, E., Yilmaz, M.T., 2021. Intercomparison of the expected change in the temperature and the precipitation retrieved from CMIP6 and CMIP5 climate projections: a mediterranean hot spot case, Turkey. Atmos. Res. 256, 105576 https://doi.org/10.1016/j.atmosres.2021.105576.

Baker, N.C., Huang, H.P., 2014. A comparative study of precipitation and evaporation between CMIP3 and CMIP5 climate model ensembles in semiarid regions. J. Clim. 27, 3731–3749. https://doi.org/10.1175/JCLI-D-13-00398.1.

Chang, C.P., Zhuo, W., John, M., Ching-Hwang, L., 2005. Annual cycle of Southeast Asia—Maritime Continent rainfall and the asymmetric monsoon transition. J. Clim. 18, 287–301. https://doi.org/10.1175/JCLI-3257.1.

Chen, H., Sun, J., Chen, X., 2014. Projection and uncertainty analysis of global precipitation-related extremes using CMIP5 models. Int. J. Climatol. 34, 2730–2748. https://doi.org/10.1002/joc.3871.

Chen, C.-A., Hsu, H.-H., Liang, H.-C., 2021. Evaluation and comparison of CMIP6 and CMIP5 model performance in simulating the seasonal extreme precipitation in the Western North Pacific and East Asia. Weather Clim. Extrem. 31, 100303 https://doi.org/10.1016/j.wace.2021.100303.

Deng, X., Perkins-Kirkpatrick, S.E., Lewis, S.C., Ritchie, E.A., 2021. Evaluation of extreme temperatures over Australia in the historical simulations of CMIP5 and CMIP6 models. Earth's Futur. 9, e2020EF001902 https://doi.org/10.1029/2020EF001902.

Desmet, Q., Ngo-Duc, T., 2021. A novel method for ranking CMIP6 global climate models over the southeast Asian region. Int. J. Climatol. 1–21 https://doi.org/10.1002/joc.7234.

Dewi, Retno Gumilang, 2010. Indonesia second national communication under the United Nations Framework Convention on Climate Change (UNFCCC). Ministry of Environment, Republic of Indonesia.

Eyring, V., Bony, S., Meehl, G.A., Senior, C.A., Stevens, B., Stouffer, R.J., Taylor, K.E., 2016. Overview of the coupled model intercomparison project phase 6 (CMIP6) experimental design and organization. Geosci. Model Dev. 9, 1937–1958. https://doi.org/10.5194/gmd-9-1937-2016.

Flato, G., Marotzke, J., Abiodun, B., Braconnot, P., Chou, S.C., Collins, W., Cox, P., Driouech, F., Emori, S., Eyring, V., 2013. Climate change 2013: the physical science basis. Contribution of working group i to the fifth assessment report of the intergovernmental panel on climate change. In: Stock, T.F., Qin, D., Plattner, G.-K., Tignor, M., Allen, S.K., Boschung, J., et al. (Eds.), Eval. Clim. Model. Cambridge Cambridge Univ. Press.

Gao, J., Sheshukov, A.Y., Yen, H., Douglas-Mankin, K.R., White, M.J., Arnold, J.G., 2019. Uncertainty of hydrologic processes caused by bias-corrected CMIP5 climate change projections with alternative historical data sources. J. Hydrol. 568, 551–561. https://doi.org/10.1016/j.jhydrol.2018.10.041.

Ge, F., Zhu, S., Peng, T., Zhao, Y., Sielmann, F., Fraedrich, K., Zhi, X., Liu, X., Tang, W., Ji, L., 2019. Risks of precipitation extremes over Southeast Asia: does 1.5 °c or 2 °c global warming make a difference? Environ. Res. Lett. 14 https://doi.org/10.1088/1748-9326/aaff7e.

Gupta, H.V., Kling, H., Yilmaz, K.K., Martinez, G.F., 2009. Decomposition of the mean squared error and NSE performance criteria: Implications for improving hydrological modelling. J. Hydrol. 377, 80–91. https://doi.org/10.1016/j.jhydrol.2009.08.003.

Gusain, A., Ghosh, S., Karmakar, S., 2020. Added value of CMIP6 over CMIP5 models in simulating Indian summer monsoon rainfall. Atmos. Res. 232, 104680 https://doi.org/10.1016/j.atmosres.2019.104680.

Hamed, M.M., Nashwan, M.S., Shahid, S., 2021a. Intercomparison of Historical Simulation and Future Projection of Rainfall and Temperature by CMIP5 and CMIP6 GCMs over Egypt.

Hamed, M.M., Nashwan, M.S., Shahid, S., 2021b. Performance evaluation of reanalysis precipitation products in Egypt using fuzzy entropy time series similarity analysis. Int. J. Climatol. 41, 5431–5446. https://doi.org/10.1002/joc.7286.

Hartmann, D.L., 2016. Chapter 11. In: Hartmann, D.L.B.T.-G.P.C. (Ed.), Global Climate Models, Second E. Elsevier, Boston, pp. 325–360. https://doi.org/10.1016/B978-0-12-328531-7.00011-6.

Hersbach, H., Bell, B., Berrisford, P., Hirahara, S., Horányi, A., Muñoz-Sabater, J., Nicolas, J., Peubey, C., Radu, R., Schepers, D., Simmons, A., Soci, C., Abdalla, S., Abellan, X., Balsamo, G., Bechtold, P., Biavati, G., Bidlot, J., Bonavita, M., De Chiara, G., Dahlgren, P., Dee, D., Diamantakis, M., Dragani, R., Flemming, J., Forbes, R., Fuentes, M., Geer, A., Haimberger, L., Healy, S., Hogan, R.J., Hólm, E., Janisková, M., Keeley, S., Laloyaux, P., Lopez, P., Lupu, C., Radnoti, G., de Rosnay, P., Rozum, I., Vamborg, F., Villaume, S., Thépaut, J.-N., 2020. The ERA5 global reanalysis. Q. J. R. Meteorol. Soc. 146, 1999–2049. https://doi.org/10.1002/qj.3803.

IPCC, 2007. Climate Change 2007-the Physical Science Basis: Working Group I Contribution to the Fourth Assessment Report of the IPCC.

Iqbal, Z., Shahid, S., Ahmed, K., Ismail, T., Ziarh, G.F., Chung, E.-S., Wang, X., 2021. Evaluation of CMIP6 GCM rainfall in mainland Southeast Asia. Atmos. Res. 254, 105525 https://doi.org/10.1016/j.atmosres.2021.105525.

Jain, S., Salunke, P., Mishra, S.K., 2019. Advantage of NEX-GDDP over CMIP5 and CORDEX data: Indian summer monsoon. Atmos. Res. 228 https://doi.org/10.1016/j.atmosres.2019.05.026.

Jiang, J.H., Su, H., Wu, L., Zhai, C., Schiro, K.A., 2021. Improvements in cloud and water vapor simulations over the tropical oceans in CMIP6 compared to CMIP5. Earth Sp. Sci. 8, e2020EA001520 https://doi.org/10.1029/2020EA001520.

Kamruzzaman, M., Shahid, S., Islam, A.R.M.T., Hwang, S., Cho, J., Zaman, M.A.U., Ahmed, M., Rahman, M.M., Hossain, M.B., 2021. Comparison of CMIP6 and CMIP5 model performance in simulating historical precipitation and temperature in Bangladesh: a preliminary study. Theor. Appl. Climatol. 145, 1385–1406.

Kang, S., Im, E.S., Eltahir, E.A.B., 2019. Future climate change enhances rainfall seasonality in a regional model of western Maritime Continent. Clim. Dyn. 52, 747–764. https://doi.org/10.1007/s00382-018-4164-9.

Khadka, D., Babel, M.S., Abatan, A.A., Collins, M., 2021. An evaluation of CMIP5 and CMIP6 climate models in simulating summer rainfall in the Southeast Asian monsoon domain. Int. J. Climatol. https://doi.org/10.1002/joc.7296 n/a.

Khan, N., Pour, S.H., Shahid, S., Ismail, T., Ahmed, K., Chung, E.S., Nawaz, N., Wang, X., 2019. Spatial distribution of secular trends in rainfall indices of Peninsular Malaysia in the presence of long-term persistence. Meteorol. Appl. 26, 655–670. https://doi.org/10.1002/met.1792.

Kling, H., Fuchs, M., Paulin, M., 2012. Runoff conditions in the upper Danube basin under an ensemble of climate change scenarios. J. Hydrol. 424–425, 264–277. https://doi.org/10.1016/j.jhydrol.2012.01.011.

Knoben, W.J.M., Freer, J.E., Woods, R.A., 2019. Technical note: inherent benchmark or not? Comparing Nash-Sutcliffe and Kling-Gupta efficiency scores. Hydrol. Earth Syst. Sci. Discuss. 1–7 https://doi.org/10.5194/hess-2019-327.

Lee, H.M., Yoo, D.G., Kim, J.H., Kang, D., Min, L.H., Do Guen, Y., Hoon, K.J., Doosun, K., 2017. Hydraulic simulation techniques for water distribution networks to treat pressure deficient conditions. J. Water Resour. Plan. Manag. 144, 07017008. https://doi.org/10.1061/(asce)wr.1943-5452.0000899.

Li, X.-X., 2020. Heat wave trends in Southeast Asia during 1979–2018: the impact of humidity. Sci. Total Environ. 721 https://doi.org/10.1016/j.scitotenv.2020.137664.

Lun, Y., Liu, L., Cheng, L., Li, X., Li, H., Xu, Z., 2021. Assessment of GCMs simulation performance for precipitation and temperature from CMIP5 to CMIP6 over the Tibetan Plateau. Int. J. Climatol. 41, 3994–4018. https://doi.org/10.1002/joc.7055.

Luo, N., Guo, Y., Chou, J., Gao, Z., 2021. Added value of CMIP6 models over CMIP5 models in simulating the climatological precipitation extremes in China. Int. J. Climatol. https://doi.org/10.1002/joc.7294 n/a.

McSweeney, C.F., Jones, R.G., Lee, R.W., Rowell, D.P., 2015. Selecting CMIP5 GCMs for downscaling over multiple regions. Clim. Dyn. 44, 3237–3260. https://doi.org/10.1007/s00382-014-2418-8.

Moss, R.H., Edmonds, J.A., Hibbard, K.A., Manning, M.R., Rose, S.K., van Vuuren, D.P., Carter, T.R., Emori, S., Kainuma, M., Kram, T., Meehl, G.A., Mitchell, J.F.B., Nakicenovic, N., Riahi, K., Smith, S.J., Stouffer, R.J., Thomson, A.M., Weyant, J.P., Wilbanks, T.J., 2010. The next generation of scenarios for climate change research and assessment. Nature 463, 747–756. https://doi.org/10.1038/nature08823.

Muhammad, M.K.I., Nashwan, M.S., Shahid, S., Ismail, T. Bin, Song, Y.H., Chung, E.S., 2019. Evaluation of empirical reference evapotranspiration models using compromise programming: a case study of Peninsular Malaysia. Sustain. 11 https://doi.org/10.3390/su11164267.

Nashwan, M.S., Shahid, S., 2022. Future precipitation changes in Egypt under the 1.5 and 2.0°C global warming goals using CMIP6 multimodel ensemble. Atmos. Res. 265, 105908 https://doi.org/10.1016/j.atmosres.2021.105908.

Nashwan, M.S., Ismail, T., Ahmed, K., 2018a. Flood susceptibility assessment in Kelantan river basin using copula. Int. J. Eng. Technol. 7, 584–590. https://doi.org/10.14419/ijet.v7i2.8876.

Nashwan, M.S., Shahid, S., Chung, E.S., Ahmed, K., Song, Y.H., 2018b. Development of climate-based index for hydrologic hazard susceptibility. Sustain. 10 https://doi.org/10.3390/su10072182.

Nasional, Badan Perencanaan Pembangunan, 2012. National Action Plan for Climate Change Adaptation (RAN-API). Jakarta: Bappenas, Indonesia.

Noor, M., Ismail, T., Shahid, S., Nashwan, M.S., Ullah, S., 2019. Development of multi-model ensemble for projection of extreme rainfall events in Peninsular Malaysia. Hydrol. Res. 50, 1772–1788. https://doi.org/10.2166/nh.2019.097.

O'Neill, B.C., Tebaldi, C., van Vuuren, Eyring, V., Friedlingstein, P., Hurtt, G., et al., 2016. The Scenario Model Intercomparison Project (ScenarioMIP) for CMIP6. Geosci. Model Dev. 9 (9), 3461–3482. https://doi.org/10.5194/gmd-9-3461-2016.

Ortega, G., Arias, P.A., Villegas, J.C., Marquet, P.A., Nobre, P., 2021. Present-day and future climate over central and South America according to CMIP5/CMIP6 models. Int. J. Climatol. https://doi.org/10.1002/joc.7221 n/a.

Peel, M.C., Finlayson, B.L., McMahon, T.A., 2007. Updated world map of the Köppen-Geiger climate classificatio. Hydrol. Earth Syst. Sci. 11, 1633–1644. https://doi.org/10.1002/ppp.421.

Qian, J.H., 2008. Why precipitation is mostly concentrated over islands in the maritime continent. J. Atmos. Sci. 65, 1428–1441. https://doi.org/10.1175/2007JAS2422.1.

Radcliffe, D.E., Mukundan, R., 2017. PRISM vs. CFSR precipitation data effects on calibration and validation of SWAT models. J. Am. Water Resour. Assoc. 53, 89–100. https://doi.org/10.1111/1752-1688.12484.

Raghavan, S.V., Vu, M.T., Liong, S.Y., 2017. Ensemble climate projections of mean and extreme rainfall over Vietnam. Glob. Planet. Chang. 148, 96–104. https://doi.org/10.1016/j.gloplacha.2016.12.003.

Robertson, A.W., Moron, V., Qian, J.-H., Chang, C.-P., Tangang, F., Aldrian, E., Koh, T.Y., Liew, J., 2011. The maritime continent monsoon. In: The Global Monsoon System, World Scientific Series on Asia-Pacific Weather and Climate. WORLD SCIENTIFIC, pp. 85–98. https://doi.org/10.1142/9789814343411_0006.

Salman, S.A., Nashwan, M.S., Ismail, T., Shahid, S., 2020. Selection of CMIP5 general circulation model outputs of precipitation for peninsular Malaysia. Hydrol. Res. 51, 781–798. https://doi.org/10.2166/nh.2020.154.

Sardeshmukh, P.D., Compo, G.P., Penland, C., 2000. Changes of probability associated with El Nino. J. Clim. 13, 4268–4286.

Schlund, M., Lauer, A., Gentine, P., Sherwood, S.C., Eyring, V., 2020. Emergent constraints on Equilibrium Climate Sensitivity in CMIP5 : do they hold for CMIP6 ? Earth Syst. Dyn. 1–40 https://doi.org/10.5194/esd-2020-49.

Shahid, S., 2010. Probable impacts of climate change on public health in Bangladesh. Asia-Pacific J. Public Heal. 22, 310–319. https://doi.org/10.1177/1010539509335499.

Shahid, S., Pour, S.H., Wang, X., Shourav, S.A., Minhans, A., Ismail, T. Bin, 2017. Impacts and adaptation to climate change in Malaysian real estate. Int. J. Clim. Chang. Strateg. Manag. 9, 87–103. https://doi.org/10.1108/IJCCSM-01-2016-0001.

Song, Y.H., Chung, E.-S., Shahid, S., 2021a. Spatiotemporal differences and uncertainties in projections of precipitation and temperature in South Korea from CMIP6 and

CMIP5 general circulation models. Int. J. Climatol. https://doi.org/10.1002/joc.7159 n/a.

Song, Y.H., Nashwan, M.S., Chung, E.S., Shahid, S., 2021b. Advances in CMIP6 INM-CM5 over CMIP5 INM-CM4 for precipitation simulation in South Korea. Atmos. Res. 247, 105261 https://doi.org/10.1016/j.atmosres.2020.105261.

Supari, Tangang, F., Juneng, L., Cruz, F., Chung, J.X., Ngai, S.T., Salimun, E., Mohd, M.S. F., Santisirisomboon, J., Singhruck, P., PhanVan, T., Ngo-Duc, T., Narisma, G., Aldrian, E., Gunawan, D., Sopaheluwakan, A., 2020. Multi-model projections of precipitation extremes in Southeast Asia based on CORDEX-Southeast Asia simulations. Environ. Res. 184, 109350 https://doi.org/10.1016/j.envres.2020.109350.

Supharatid, S., Nafung, J., Aribarg, T., 2021. Projected changes in temperature and precipitation over mainland Southeast Asia by CMIP6 models. J. Water Clim. Chang. 1–20 https://doi.org/10.2166/wcc.2021.015.

Tangang, F., Chung, J.X., Juneng, L., Supari, Salimun, E., Ngai, S.T., Jamaluddin, A.F., Mohd, M.S.F., Cruz, F., Narisma, G., Santisirisomboon, J., Ngo-Duc, T., Van Tan, P., Singhruck, P., Gunawan, D., Aldrian, E., Sopaheluwakan, A., Grigory, N., Remedio, A.R.C., Sein, D.V., Hein-Griggs, D., McGregor, J.L., Yang, H., Sasaki, H., Kumar, P., 2020. Projected future changes in rainfall in Southeast Asia based on CORDEX–SEA multi-model simulations. Clim. Dyn. 55, 1247–1267. https://doi.org/10.1007/s00382-020-05322-2.

Taylor, K.E., 2001. Summarizing multiple aspects of model performance in a single diagram. J. Geophys. Res. Atmos. 106, 7183–7192. https://doi.org/10.1029/2000JD900719.

Taylor, K.E., Balaji, V., Hankin, S., Juckes, M., Lawrence, B., Pascoe, S., 2011. CMIP5 Data Reference Syntax (DRS) and Controlled Vocabularies. San Francisco Bay Area, CA, USA.

Taylor, M.A., Clarke, L.A., Centella, A., Bezanilla, A., Stephenson, T.S., Jones, J.J., Campbell, J.D., Vichot, A., Charlery, J., 2018. Future Caribbean climates in a world of rising temperatures: The 1.5 vs 2.0 dilemma. J. Clim. 31, 2907–2926.

Taylor, K.E., Stouffer, R.J., Meehl, G.A., 2012. An overview of CMIP5 and the experiment design. Bull. Am. Meteorol. Soc. 93, 485–498. https://doi.org/10.1175/BAMS-D-11-00094.1.

Thirumalai, K., DiNezio, P.N., Okumura, Y., Deser, C., 2017. Extreme temperatures in Southeast Asia caused by El Niño and worsened by global warming. Nat. Commun. 8, 15531. https://doi.org/10.1038/ncomms15531.

van Vuuren, D.P., Edmonds, J., Kainuma, M., Riahi, K., Thomson, A., Hibbard, K., Hurtt, G.C., Kram, T., Krey, V., Lamarque, J.-F., Masui, T., Meinshausen, M., Nakicenovic, N., Smith, S.J., Rose, S.K., 2011. The representative concentration pathways: an overview. Clim. Chang. 109, 5. https://doi.org/10.1007/s10584-011-0148-z.

Weigel, A.P., Knutti, R., Liniger, M.A., Appenzeller, C., 2010. Risks of model weighting in multimodel climate projections. J. Clim. 23, 4175–4191. https://doi.org/10.1175/2010JCLI3594.1.

Yang, S., Wu, R., Jian, M., Huang, J., Hu, X., Wang, Z., Jiang, X., 2021. Climate Change in Southeast Asia and Surrounding Areas. Springer Climate.

Yazdandoost, F., Moradian, S., Izadi, A., Aghakouchak, A., 2021. Evaluation of CMIP6 precipitation simulations across different climatic zones: uncertainty and model intercomparison. Atmos. Res. 250, 105369 https://doi.org/10.1016/j.atmosres.2020.105369.

Yoneyama, K., Zhang, C., 2020. Years of the Maritime Continent. Geophys. Res. Lett. 47, e2020GL087182 https://doi.org/10.1029/2020GL087182.

Zhai, J., Mondal, S.K., Fischer, T., Wang, Y., Su, B., Huang, J., Tao, H., Wang, G., Ullah, W., Uddin, M.J., 2020. Future drought characteristics through a multi-model ensemble from CMIP6 over South Asia. Atmos. Res. 246, 105111 https://doi.org/10.1016/j.atmosres.2020.105111.

Zhu, X., Lee, S.-Y., Wen, X., Ji, Z., Lin, L., Wei, Z., Zheng, Z., Xu, D., Dong, W., 2021. Extreme climate changes over three major river basins in China as seen in CMIP5 and CMIP6. Clim. Dyn. https://doi.org/10.1007/s00382-021-05767-z.

Ziarh, G.F., Asaduzzaman, M., Dewan, A., Nashwan, M.S., Shahid, S., 2021. Integration of catastrophe and entropy theories for flood risk mapping in peninsular Malaysia. J. Flood Risk Manag. 14, e12686 https://doi.org/10.1111/jfr3.12686.

Zuluaga, C.F., Avila-Diaz, A., Justino, F.B., Wilson, A.B., 2021. Climatology and trends of downward shortwave radiation over Brazil. Atmos. Res. 250, 105347 https://doi.org/10.1016/j.atmosres.2020.105347.